

This is the **accepted version** of the journal article:

Paredes, Ferran; Moya Lara, Ana; Berenguel-Alonso, Miguel; [et al.]. «Motion Control System for Industrial Scenarios Based on Electromagnetic Encoders». iEEE Transactions on Instrumentation and Measurement, Vol. 72 (May 2023). DOI 10.1109/TIM.2023.3271758

This version is available at <https://ddd.uab.cat/record/275095>

under the terms of the  ^{IN}
COPYRIGHT license

Motion Control System for Industrial Scenarios Based on Electromagnetic Encoders

Ferran Paredes, *Senior Member, IEEE*, Ana Moya, Miguel Berenguel-Alonso, David Gonzalez, Pep Bruguera, Claudia Delgado-Simao, and Ferran Martín, *Fellow, IEEE*

Abstract— In this paper, a complete system useful for the measurement of the absolute position, velocity, and acceleration of moving objects in industrial scenarios (such as conveyor transport devices, elevators, escalators, and other mechanical systems) is presented. The proposed system contains an electromagnetic encoder consisting of a pair of chains of metallic patches screen-printed on a rubber belt. In one of the chains (designated as clock/velocity chain), the patches are printed at predefined periodic positions. Such clock chain generates also the clock signal necessary to read the other chain (position chain), with patches either present (binary state ‘1’) or absent (binary state ‘0’) at their predefined positions. The system includes a reader based on a transmission line with three resonators etched on the ground plane and fed with three harmonic signals. Such three elements are complementary split ring resonators (CSRRs), which are sensitive to the presence of patches at short distance on top of them, and therefore they are used to detect the patches as the encoder moves with regard to the reader. By encoder motion, the patches generate three amplitude modulation (AM) signals, providing the velocity (and acceleration), the absolute encoder position, and the motion direction. A prototype system, including the encoder, the reader and the associated electronics is designed, fabricated and validated.

Index Terms— Electromagnetic encoders, position sensors, microwave sensors, motion control, printed electronics, microwave technology

I. INTRODUCTION

WITHIN the framework of the 4.0 Industry, there is an increasing demand of systems devoted to the so-called motion control. There are many industrial mechanical systems that require position and velocity control, including servomotors, conveyor transport systems, pointing mechanisms, elevators, escalators, etc. Usually, motion control

systems include a feedback loop, where position sensors are required, in order to compensate for potential errors between controllers and actuators (e.g., a step motor).

One of the most extended technologies for motion control sensors is optics [1]-[3]. Thus, optical encoders are used to accurately determine the position, velocity and acceleration of moving systems, such as conveyor belts or elevators, among many others. In optical rotary encoders, the angular position, velocity, and acceleration is measured from a set of pulsed signals recorded with an optical detector, and then digitally post-processed. The encoders are made of a metallic, glass, or plastic disc with apertures arranged in series. A source generates an optical beam, and a photodetector detects pulses obtained by the presence or absence of encoder apertures. Certain optical rotary encoders exhibit several thousands of pulses per cycle, thereby providing sub-degree angle resolutions.

Despite their high resolution, optical encoders may find limitations in environments where pollution, dirtiness, grease, radiation, etc. are present. Microwaves offer an alternative approach for the implementation of displacement (either angular or linear) and velocity sensors, which may result interesting in scenarios subjected to severe and harsh conditions (microwave systems are, in general, robust against the pernicious effects of such hostile conditions). Thus, microwave (or electromagnetic) rotary encoders have been recently reported [4]-[8]. Such encoders exhibit good angular resolution (e.g., 0.3° in the encoders reported in [7]), and an unlimited dynamic range, in comparison with other microwave angular displacement and microwave velocity sensors [9]-[17].

The functionality of microwave encoders is analogous to the functionality of optical encoders. In microwave encoders, the metallic inclusions (etched or printed on a dielectric substrate) are used instead of the apertures, and such inclusions are either arranged in the outer edge of a disc, or rotor (rotary encoders), forming circular chains [4]-[8], or linearly distributed along the movable element of the motion sensor, forming linear chains (linear encoders) [18],[19]. Nevertheless, microwave encoders based on all-dielectric inclusions (either low or high permittivity constant materials) have been recently reported [20],[21].

In electromagnetic encoders, the inclusions (metallic or dielectric) are detected through their effects on a microwave signal propagating in a transmission line, with a resonator etched on the ground plane. This resonator-loaded line

This work was supported by MCIN/AEI 10.13039/501100011033, Spain, through the projects PID2019-103904RB-I00 (ERDF European Union), RTC-2017-6303-7 (ERDF European Union), and PDC2021-121085-I00 (European Union Next Generation EU/PRTR), by the AGAUR Research Agency, Catalonia Government, through the project 2021SGR-00192, and by Institució Catalana de Recerca i Estudis Avançats (who awarded Ferran Martín).

F. Paredes and F. Martín are with CIMITEC, Departament d'Enginyeria Electrònica, Universitat Autònoma de Barcelona, 08193 Bellaterra, Spain (e-mail: Ferran.Martin@uab.cat).

A. Moya, M. Berenguel-Alonso and C. Delgado-Simao are with T. Eurecat, Centre Tecnològic de Catalunya, Parc Científic i de la Innovació Tecno Campus, 08302 Mataró, Spain (e-mail: claudia.delgado@eurecat.org).

D. González and P. Bruguera are with Hohner Automation, P.I. Cal Batlle, 17400 Breda, Spain (e-mail: bruguera@encoderhohner.com).

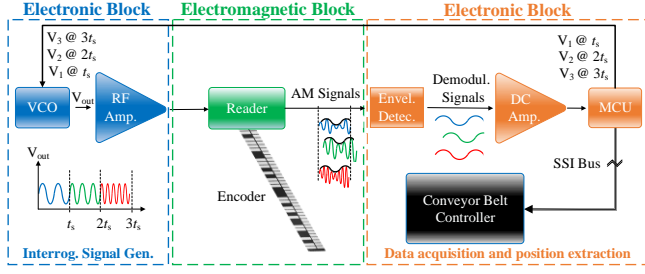


Fig. 1. Schematic of the motion control system for the measurement of encoder position, velocity, and direction.

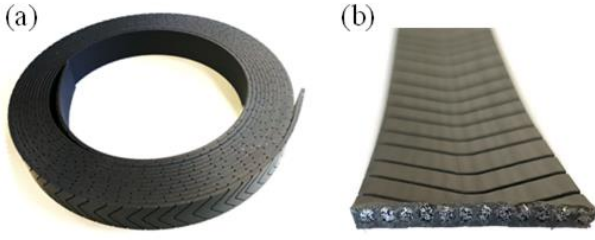


Fig. 2. Photograph of a commercial elevator belt (a) and detail of the cross section (b).

constitutes the sensitive part of the reader, which is the static part of the motion sensor, and is designated as stator in rotary encoders. The presence of encoder inclusions close to the loading resonator modifies its resonance frequency (and hence a variation in the transmission coefficient), so that the velocity and position can be inferred [5]. In general terms, there are two types of microwave encoders: the incremental-type [7] and the absolute-type microwave encoder [22]. The latter are preferred because they are able to provide the relative position between the reader and the encoder after a system reset. However, in the absolute-type encoders it is required at least two chains of inclusions, one devoted to the determination of the velocity (and acceleration) and motion direction, and another one used to infer the absolute position, following a certain sequence (details are given later). In the chain dedicated to obtaining the velocity, the inclusions must be set at equidistant (periodic) positions.

In this work, it is demonstrated that the preliminary system first reported in [22] can potentially be applied to the determination of the absolute position, velocity (and acceleration), and motion direction of moving objects in industrial systems (e.g., conveyor transport systems or elevators). As a first step, the functionality of microwave encoders, where the metallic patches were screen-printed on rubber belts, was demonstrated in [23]. In this work, the whole system, including the associated electronics for generating the signals, as well as the post-processing stage, is reported. Moreover, system functionality is demonstrated through a prototype that emulates an actual industrial system (i.e., the validation of the proposed linear encoder system is closer to operational environment). As it will be shown later (Section IV), all the electronics (in charge of generating and processing

the resulting data and finally obtaining the position) have been included in a PCB, this representing a novel aspect as compared to [23]. Let us also mention that, in this paper, a number of tests/studies to analyze the robustness of the system has been conducted. This includes an analysis about the effects of the number of ink layers and dielectric (protective) coating of the encoders on the repeatability of the reader responses, as well as various environmental and stress tests. Such tests include mechanical traction and mechanical bending of the encoders, subjecting them to different humidity conditions and temperatures, and a corrosion test (by applying saline salt spray).

The manuscript is organized as follows. The system concept is described in Section II, which includes the specificities of the proposed encoders (two linear columns of metallic patches) and reader (a microstrip line loaded with three complementary split ring resonators -CSRRs) [24]. Section III is devoted to encoder and reader fabrication. Such section also reports the results of several tests carried out on the fabricated encoders, in order to ensure their robustness against extreme operating conditions. The validation of the system is presented in Section IV, where the experimental prototype and the necessary reader electronics are described in detail. Finally, the main conclusions are highlighted in Section V.

II. SYSTEM CONCEPT AND PROPOSED READER AND ENCODER

The schematic of the conceived system for the measurement of the position, velocity, acceleration and motion direction of the encoder belt is depicted in Fig. 1. The considered material for encoder implementation is rubber, a dielectric material present in many industrial systems, such as elevators (elevator belts), or conveyor systems (conveyor belts), among others. In particular, in this paper we have considered a commercial elevator belt, since validation of encoder functionality using such (rubber) material as substrate for screen-printing the encoder patterns (an aspect to be latter justified) is a demonstration of the potentiality of the approach under consideration. The reason is that the dielectric and mechanical properties of rubber cannot compete against those of other polymeric or ceramic materials that can also be used as substrate for encoder implementation. Thus, encoder validation in belts made of rubber (a non-favorable material but encountered in many industrial systems) is meaningful. Moreover, elevator belts contain several metallic cores in order to support the weight of the cabin (Fig. 2), thereby adding an extra difficulty to the functionality of the system when such belts are used as encoders. Since the cross-sectional geometry of elevator belts is rectangular, with an extreme shape factor, it is potentially possible to screen-print the required metallic encoder patterns (a chain or various chains of metallic inclusions) along the entire length of the belt (on the wider face of it). The expected result is a microwave encoder implemented in a commercially available substrate (elevator belt), as a case example representative of many other similar materials that can be found in industry.

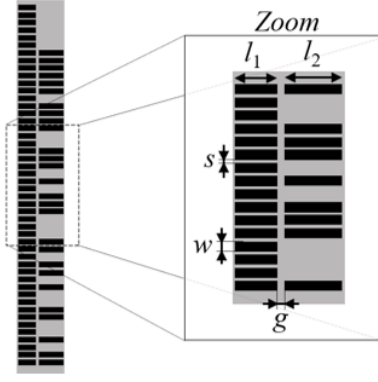


Fig. 3. Layout of the proposed encoder. Dimensions (in mm) are: $l_1 = 11.5$, $l_2 = 15.9$, $w = 3$, $s = 1$ and $g = 1.9$.

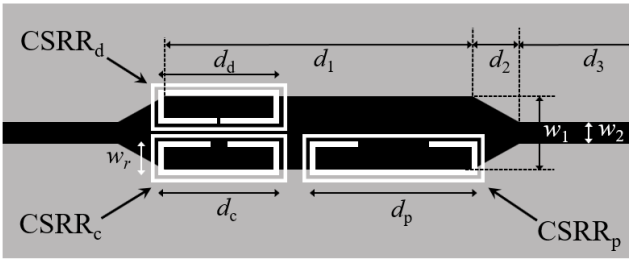


Fig. 4. Topology of the sensitive part of the reader. Dimensions (in mm) are: $d_1 = 26.6$; $d_2 = 3.8$, $d_3 = 10$, $w_1 = 6.4$, $w_2 = 1.9$, $d_c = d_d = 10.5$; $d_p = 14.5$, $w_r = 2.9$. The CSRR dimensions (in mm) are: slots width $c = 0.5$ and ring splits $s_d = 0.4$, $s_c = 1.6$ and $s_p = 6.2$.

Concerning the reader, it must be located in a position in close proximity to the belt, as far as the detection of inclusions, necessary for encoder reading, must be carried out by proximity [22].

The required functionality of the system must include the measurement of the absolute encoder position, as well as the encoder velocity and acceleration. Moreover, the system must be able to give the motion direction of the microwave encoder. For that purpose, the encoder must be equipped with two chains. One of the chains, designated as clock chain in this paper, is made of rectangular metallic patches screen-printed on the elevator belt at periodic positions. This chain provides the instantaneous velocity and acceleration, obtained from the distances between adjacent time pulses in the envelope function (to be discussed later). Moreover, this chain acts as a synchronous chain (i.e., it provides the clock signal), required to detect the instants of time to read the second (codified) chain in a synchronous reading scheme. Finally, the clock chain also provides the direction of motion, determined from the lag or lead of the clock signal when compared with a redundant signal (as it will be shown). The second chain, designated as position chain, contains a certain ID code and is used to determine the absolute position of the cabin. The binary state, '1' or '0', at each predefined position is determined by the presence or absence, respectively, of a rectangular patch.

In order to obtain the absolute position of the microwave encoder, the reader determines the binary states of the position chain sequentially, at the instants of time dictated by the clock signal. The position is given by the corresponding bit inferred at that position, plus the previous $N - 1$ bits of the chain. Thus, such N -bit sub-sequence univocally determines the cabin position. Obviously, with this approach, it is necessary that any N -bit sub-code of the whole encoder (with all bits consecutive) is different. To guarantee this, i.e., that any N -bit sub-code is assigned to a different cabin position, the bit sequence of the whole encoder (position chain) must be selected according to the De Bruijn theorem [25]. The main relevant characteristic of this sequence is that any N -bit sub-code does not repeat for the total set of cabin positions.

Let us designate by L the length of the whole position chain (identical to the length of the clock chain), and by p the period of the chains (referred to the predefined locations in the position chain). The abovementioned period is an elemental parameter, as it determines the spatial resolution of the system. The number of different positions of the encoder is given by the ratio L/p . Therefore, the number of bits, N , of the sub-code necessary to univocally provide the cabin position must comply with

$$N \geq \log_2 \left(\frac{L}{p} \right) \quad (1)$$

It is worth mentioning that two different N -bit sub-code sequences are needed for both directions of motion (e.g., upper and lower motion). With this system, when there is a change in the direction of motion (or after a system reset), it is necessary that the encoder displaces a distance corresponding to N positions, in order to read the N bits of the sub-code that are needed to determine the absolute position from the table. This "after-reset uncertainty" is consequence of the fact that a single bit is assigned to each encoder position (i.e., a unique position chain is used).

The layout of the microwave encoder is shown in Fig. 3, along with the whole dimensions. The reader layout is depicted in Fig. 4. The period (and hence the spatial resolution) is $p = 4$ mm. Let us consider, for instance, that the total length of the encoder in a real scenario (e.g., an elevator system) is 20 m. According to (1), the sub-code sequences must contain at least $N = 13$ bits. For demonstration purposes at laboratory level, however, we will consider an encoder of length $L = 20$ cm (Fig. 3). At the edges of the encoder, 4-mm margins have been considered, so that 48 metallic patches (i.e., 48 bits) have been screen-printed. This corresponds to a subset of $N = 6$ bits. The details of encoder fabrication are given in Section III. With magnetic and inductive encoders [26,27] very good resolutions can be achieved, but at the expense of using magnets or coils.

Let us now center the discussion on the reader, consisting of the transmission line with three resonators (CSRRs) etched in the ground plane and tuned to different frequencies (Fig. 4). Each CSRR is used for a different purpose. Thus, the resonator designated as CSRR_p is used to determine the encoder position, and consequently it may be located beneath

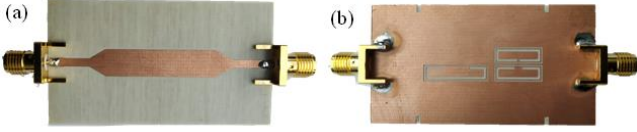


Fig. 5. Photograph of the fabricated reader, including (a) the top and (b) the bottom views.

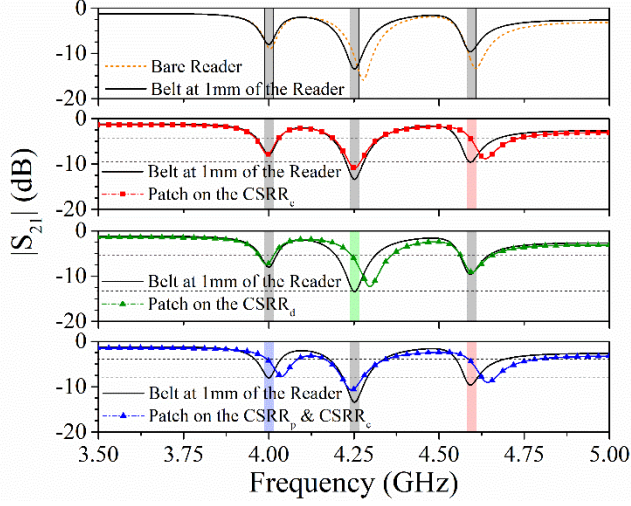


Fig. 6. The frequency response of the bare reader, reader with the conveyor belt (without any patch) located at 1mm distance on top of it, and reader selectively covered with patches on top of the different CSRRs (indicated). The patches are printed on the conveyor belt.

the position chain. Bit identification (i.e., patch detection) proceeds by generating a harmonic (interrogation) signal, operating at the same frequency of the CSRR_p , and injecting it to the line (such frequency is designated as $f_{0,p}$). If a metallic patch of the position chain is just above of the CSRR_p , it is detuned, and the transmission coefficient at $f_{0,p}$ increases dramatically. The effect is an amplitude modulation (AM) of the interrogation signal at the output port of the line, with maxima in the envelope function each time a patch crosses the position of the CSRR_p . Such envelope function contains, therefore, the ID (identification) code of the position chain, and, particularly, the N -bit sub-codes, necessary to obtain the position of the cabin.

The other two resonators, designated as CSRR_c and CSRR_d , should be located in the ground plane, aligned with the clock chain. This chain contains all the patches at their predefined positions. Therefore, when a harmonic signal is injected to the line tuned either to the operation frequency of the CSRR_c , $f_{0,c}$, or to the resonance frequency of the CSRR_d , $f_{0,d}$, an AM modulated signal with a periodic envelope function is expected at the output port of the line. Thus, the velocity of the microwave encoder can be determined from the time lapse between adjacent peaks (provided the separation between adjacent patches is well known). The acceleration is simply inferred by taking the derivative of the velocity. Note that the velocity and acceleration information can be inferred from both envelope functions, the one of the AM signal with carrier

at $f_{0,c}$ (clock signal), and the one of the AM signal with carrier at $f_{0,d}$ (redundant signal). Note that the clock signal is generated by the effects of the clock chain on the resonator designated as CSRR_c , which is transversally aligned with the resonator called CSRR_p . Therefore, it is clear that the clock signal is used to determine the instants of time for reading the position chain, following a synchronous reading scheme. The redundant AM signal, generated by the effects of the clock chain on the carrier signal tuned to $f_{0,d}$, is necessary to obtain the direction of the motion. For that purpose, it suffices to check whether the redundant signal lags or leads with respect to the clock signal, since the clock chain patches cross first the CSRR_c and then CSRR_d , or vice versa, depending on the motion direction of the encoder.

It should be mentioned that the dimensions of the patches of the clock (l_1) and position (l_2) chain are unequal (see Fig. 3). This eases the tuning of the corresponding CSRRs (CSRR_c and CSRR_p) to different frequencies. However, note that the patch dimension (w) in the direction of motion and patch separation (s) are identical in both chains (this is necessary for synchronously reading the position chain, at the rate dictated by the clock signal). The length (d_d) and width (w_r) of the CSRR_d are identical to those of the CSRR_c (d_c and w_r , respectively), since both resonators must be sensitive to identical patches (those of the clock chain). However, note that the slits of these resonators (s_d and s_c) are different, as corresponds to the fact that they are tuned to different frequencies. Note also that a ring slot surrounds the three resonators, as a means to tailor the quality factor. This is necessary in order to achieve the required excursion of the transmission coefficient (intimately related to the modulation index), as the resonators are detuned by the effects of the patches. Let us mention that, despite the fact that other slot resonators can be used to detect the presence of the encoder patches on top of them, CSRRs can be easily tuned (in frequency) and tailored, in order to exhibit a high quality factor. Moreover, the CSRR is an electrically small particle. For all these reasons, the CSRR has been the considered sensitive element of the reader in the proposed system.

According to the previous words, three independent harmonic signals are required for encoder reading. In the angular velocity sensors with motion direction detection capability reported in [7], a combiner and a diplexer were used to independently determine the information relative to the angular velocity and position (those encoders are incremental) from the one in regard to motion direction. In this work, we propose a different system, based on a VCO and a microcontroller, to be discussed in Section IV (devoted to the experimental validation).

III. READER AND ENCODER FABRICATION

With the CSRRs dimensions indicated in the caption of Fig. 4, the corresponding resonance frequencies are roughly equidistant, provided the reader substrate for fabrication is the *Rogers RO4003C* with thickness $h = 0.81$, permittivity $\epsilon_r = 3.38$, mm and loss factor $\tan\delta = 0.0022$. Figure 5 shows the

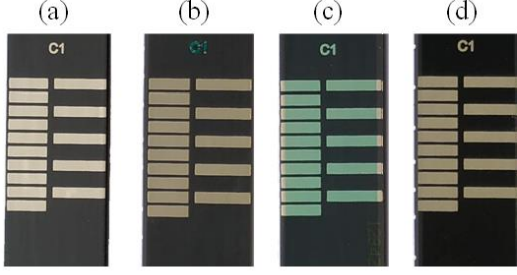


Fig. 7. Photographs of the encoders with (a) one layer, (b) two layers, (c) one layer of conductive silver ink coated with a layer of green dielectric ink, (d) one layer of conductive silver ink protected with a layer of transparent dielectric ink.

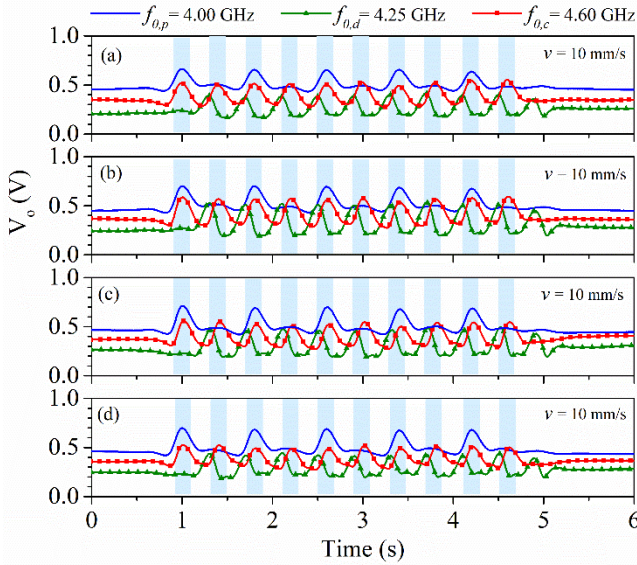


Fig. 8. Envelope functions for the three harmonic signals and for the different encoders of Fig.7 (labeled with a, b, c, and d).

fabricated reader photograph (sensitive part), whereas the measured frequency responses of the bare reader are shown in Fig. 6. The measured resonances for the CSRR_p, CSRR_d and CSRR_c resonators are found to be $f_{0,p} = 4.00$ GHz, $f_{0,d} = 4.25$ GHz and $f_{0,c} = 4.60$ GHz, respectively.

We have also obtained the measured responses that result by covering each of the CSRRs with a metallic patch (with the corresponding dimensions) screen-printed (with a single layer) on the rubber belt. The air gap (vertical distance between the reader and the metallic patches) is considered to be 1 mm in all the cases. These three measured responses, also depicted in Fig. 6, reveal that a resonance frequency shift is produced by the effects of the patch on top of the corresponding CSRR. Note that in the last case, two frequency shifts can be observed due to the synchronous nature of the proposed system, namely, when a patch is on top of the resonator devoted to determining the position, CSRR_p, necessarily there must also be a patch on top of the clock resonator, CSRR_c. These results are expected, but they verify that the frequency shift is enough, in all the

cases, to achieve a substantial magnitude variation of the transmission coefficient at the nominal resonance frequencies of the bare (uncovered) reader. This aspect is significant to provide a high modulation index in the three AM modulated signals at the output port of the reader line. A high modulation index is a requirement for system robustness against potential vibrations or misalignment between the encoder and the reader.

Concerning encoder fabrication, the first step was to demonstrate that the reader was able to correctly detect the metallic patches screen-printed on the rubber belt. Thus, in the first encoders, rather than screen-printing the clock chain and a certain (de Bruijn) position chain, we simply implemented a 10-bit encoder, with 10 patches in the clock chain and 5 patches (alternating between '1' and '0') in the position chain. The considered rubber belt was the commercial elevator belt model *Otis Gen2 AAA717W1* (with transverse dimensions of 3 cm × 0.3 cm), whereas the conductive ink was the commercial *Norcote ELG* silver ink. Indeed, several encoders were actually fabricated, i.e., with a single layer of conductive ink and with two layers, in order to test the conductivity.

For encoder fabrication, a halogen light (5 s at 500W) was employed to cure (ultra-violet) the silver ink after the screen-printing process. Later, the printed belt was put into an air flow oven (10 minutes at 130°C) to make thermal curing. After printing, the thickness and the resistance of several patches were measured to calculate the conductivity. The patch thicknesses were measured by means of a *Veeco* profilometer, obtaining values of 57.4 μm with small variations of ± 10 μm. By means of a multimeter, the resistances of those patches were measured, resulting in $1.7 \Omega \pm 0.2 \Omega$ and $0.9 \Omega \pm 0.1 \Omega$, for one layer and two layers, respectively. The conductivity resulted in 2.6×10^5 S/m and 5.2×10^5 S/m, for one layer and two layers, respectively.

Moreover, for ink protection against mechanical wearing or friction, such encoders were also coated with a dielectric material (i.e., a dielectric ink, also screen-printed). The dielectric inks used were the *Creative CFSN6061* (green color) and the *Norcote ELG-1400* (transparent). The photographs of the fabricated encoders are shown in Fig. 7.

Though system validation, including the associated electronics, is left for the next section, let us next present the effects of encoder motion over the reader, by injecting separately the three signals to the sensitive part of the microwave reader, and by considering the different fabricated encoders. The results are depicted in Fig. 8 (an envelope detector was used to retrieve the envelope functions). In view of such figure, we can conclude that the patches are able to efficiently modulate the amplitude of the injected signal for each harmonic, and, consequently, the patches can be detected with the designed and fabricated reader. Moreover, it can be appreciated, that the envelope functions are almost undistinguishable regardless of the number of ink layers of the encoder and the presence of the dielectric ink. Thus, from these results, it is clear that for encoder fabrication, one ink layer suffices, and the presence of the dielectric layer entirely coating the encoder is convenient in order to provide

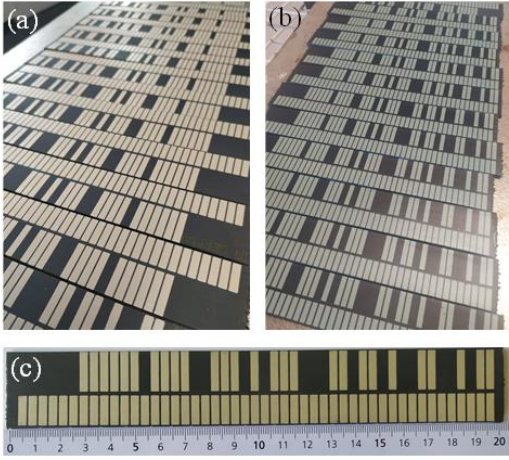


Fig. 9. Photographs of the encoders with the de Bruijn pattern printed for testing in different environments (a) with one layer of conductive silver ink, (b) with one layer of conductive silver ink protected with a layer of a green dielectric ink, and (c) conveyor belt with only one layer of conductive silver ink where the de Bruijn codification can be appreciated.

robustness against mechanics wearing or friction, as far as the effects of such layer on the encoder response are negligible.

The next step consisted in directly printing the de Bruijn code of Fig. 3 to the conveyor belts, following the same printing process mentioned before. The length of the encoder is $L = 20$ cm, whereas the period is $p = 4$ mm, so that the number of encoder positions (subset) that are necessary to univocally determine the position is $N = 6$ [see expression (1)], as anticipated before. Thus, we have generated a de Bruijn sequence such that any 6-bit subset of adjacent bits of the position chain does not repeat. This de Bruijn sequence was printed in a set of encoders (see Fig. 9), with and without (coating) dielectric inks. All these samples were printed in order to carry out a set of environmental and stress tests.

A total of nine tests were executed, including mechanical traction and mechanical bending of the encoders, subjecting them to different humidity conditions and temperatures, as well as applying saline salt spray to test the corrosion. For the mechanical traction (see Fig. 10), two different tests were carried out: (i) three repetitions of 1 hour where the belt was stressed mechanically with 3.6 kN and (ii) three repetitions of 1 hour where the belt was stressed mechanically with 52 kN. Another test consisted in (iii) bending the encoder for 24 hours within a pulley with 80 mm of radius. The belts were also tested in a climate chamber for 48 hours, where the temperatures were rising from 0°C until 80°C in 5 hours, and later decreasing back to 0°C, also for 5 hours. These tests were carried out three times for a humidity of (iv) 55 %, (v) 75 % and (vi) 95 %. Finally, the last encoders were introduced in a saline salt spray chamber with a 5 % NaCl, according to the standard *UNE EN ISO 9227*, for (vii) 24, (viii) 48 and (ix) 72 hours.

The encoders of Fig 9 were employed for all the tests, except for those tests requiring mechanical stress, which were



Fig. 10. Photographs of the encoder, with one layer of conductive silver ink coated with a layer of green dielectric ink, being stressed mechanically.

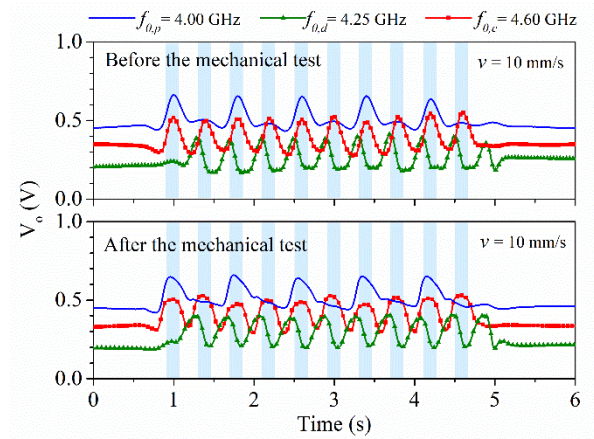


Fig. 11. Envelope functions for the encoder shown in Fig. 7(c), before and after of being stressed mechanically with 52 kN (test ii).

carried out with the encoders of Fig. 7. The reason is that, in order to apply the stress, it was necessary to hold the belt ends, and the patches at the edges (for the encoders of Fig. 9) were damaged. Figure 10 shows the belt of Fig. 7(c) subjected to mechanical stress. The belt was measured before and after the test, and the results are shown in Fig. 11. It can be appreciated that the peaks corresponding to the encoder with patches mechanically stressed have been widened somehow. However, the peaks of the three signals keep the same period and can be synchronized, and it is possible to discern the logic states of the signals. In Fig. 12, the envelope functions of the encoder of Fig. 9 before carrying out the tests are shown. After carrying out the resulting tests, all the patches, including the clock chain, as well as the position chain, were correctly read. To demonstrate this, Fig. 13 shows the envelope functions for the three harmonic signals after carrying out the test in a climate chamber for temperature and humidity variations (test vi), and the test with saline salt spray for 72 hours (test ix). It can be seen that the “1” logic states of the position chains are in good agreement with those patches present in the conveyor belt (Fig. 9c).

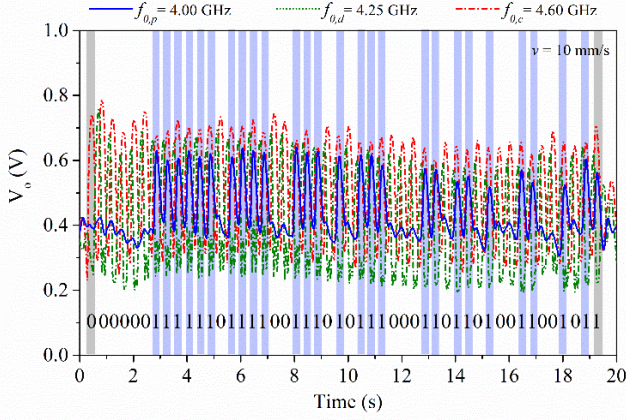


Fig. 12. Envelope functions for the three harmonic signals of the encoder of Fig. 9(c), before applying any test.

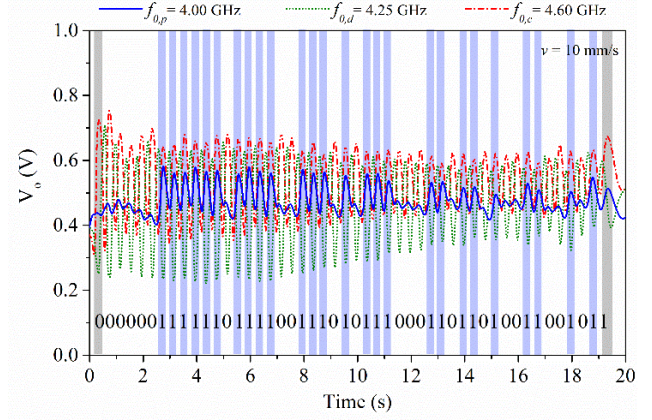


Fig. 14. Envelope functions for the encoder 9(c), when the airgap is not constant.

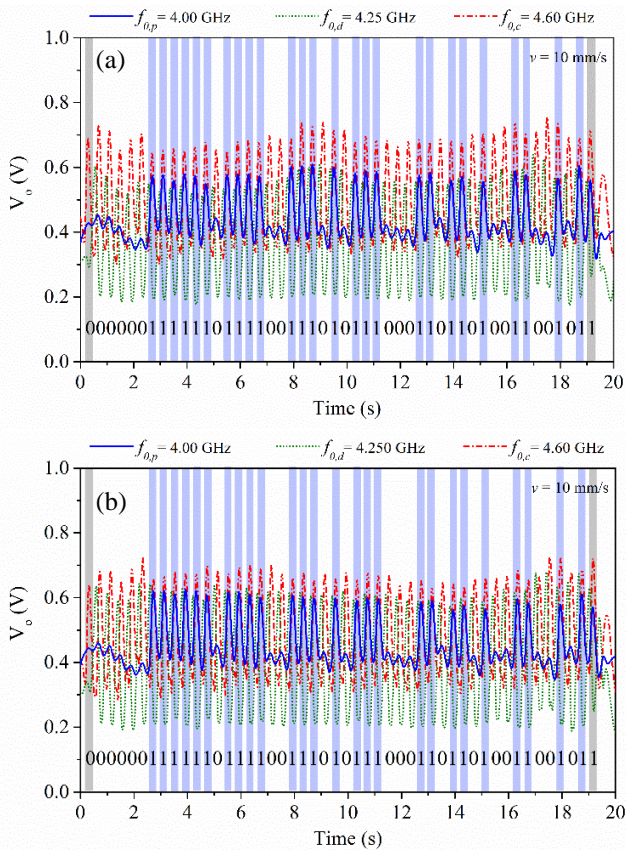


Fig. 13. Envelope functions for the three harmonic signals of the encoder of Fig. 9(c), (a) after being in a climate chamber for temperature and humidity variations (test vi), and (b) after being in a saline salt spray chamber for 72 hours (test ix).

The main cause of measurement errors during the reading stage were attributed to the lack of constant airgap or misalignments between the encoders and the reader. Increasing the airgap, directly reduces the amplitude of the signals, whereas decreasing the airgap involves major coupling between the reader and the encoder, and it can detune the operation frequencies. Thus, for soft variations of the airgap, the system will be unable to discern between the logic

states (“0” or “1”). Moreover, it is important to mention that, considering the three signals (clock, direction, and position), the position signal has the lowest amplitude and therefore, this is the most susceptible signal to measurement errors. In order to analyze the effect of fluctuation of the signal level, similar to quantify the bit error rate, or the relation to received signal to noise (SNR), we carried out a measurement where the airgap was not constant. Thus, the measurement carried out in Fig. 12, with an airgap of 1 mm, was repeated with an airgap from 1 mm to 1.5 mm (Fig. 14). In order to quantify the measurement error, an upper and lower threshold voltage was assigned to each logic state for the three signals (e.g. 0.6 V for the upper threshold level and 0.4 V for the lower threshold level, for the clock signal at $f_{0,c} = 4.60$ GHz). Since the belt contains 48 bits for the clock signal, and one bit is under the threshold, the bit error rate (BER) is 2%. The BER for the direction (0.5 V and 0.3 V for the upper and lower threshold, respectively) is 0% and the BER for the position signal (0.55 V and 0.45 V for the upper and lower threshold, respectively) is 8 %. These BERs correspond to the experiment with constant air gap of 1 mm. The calculated BER for the measurements of Fig. 14, where airgap is not constant, results in 58 %, 44 % and 60 %, for the clock, direction, and position signals, respectively. Obviously, the BERs can be reduced in the abovementioned cases if the threshold levels are properly readjusted. Thus, to avoid reading errors, the reader and the encoder were set and tightened in the linear system (section IV), and the system was always initially calibrated (first measurement in order to define the threshold voltages for the signals).

Finally, another aspect to consider for the system is the friction, or mechanical wearing. In order to test the robustness of the system, some random cuts (cracks) were applied to the patches of the encoder of Fig. 7, as shown in Fig. 15. Again, the encoder was measured before and after the generation of the cracks, and the results are shown in Fig. 16. Although, the amplitude of the peaks of the three signals has been significantly degraded, it is possible to discern the two different logic states. However, the effect of the cracks is the reduction of the coupling between the reader and the encoder patches, affecting system robustness.

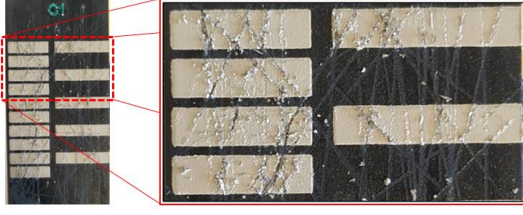


Fig. 15. Photographs of the encoder, with one layer of conductive silver ink coated, where cracks have been applied to the patches.

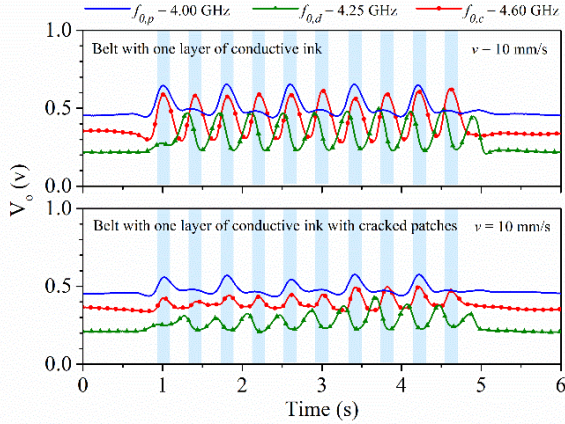


Fig. 16. Envelope functions for the encoder shown in Fig. 7(c), before and after being cracked.

IV. EXPERIMENTAL VALIDATION

The responses corresponding to the previous measured envelope functions were obtained by subsequently injecting the three harmonic signals, by means of the *Agilent N5221A* vector network analyzer employed as a signal generator, and independently retrieving the envelope function by means of a Schottky diode, an active probe and an oscilloscope. The model devices are: *Avago HSMS-2860* for the Schottky diode, the *N2795A* for the active probe, and the *Agilent MSO-X-3104A* for the oscilloscope. The encoder was displaced over the reader by using the *Thorlabs LTS300/M* linear displacement system.

In this section, we report the validation of a linear encoder system closer to operational environment. In this validation, rather than the encoder, the element in motion is the reader, but this does not represent any restriction. The air gap is estimated to be 1 mm, approximately. For system implementation, a printed circuit board, including all the electronics (in charge of generating and processing the resulting data and finally obtaining the position) was designed and fabricated. The schematic in charge of generating the signals and obtain the AM demodulation is shown in Fig. 17. For the generation of the three harmonic signals, a voltage-controlled oscillator (VCO), model *HMC391LP4*, connected by means of a coupling capacitor to the *TRF37D73* RF gain amplifier, was used. Such amplifier is connected to the input port of the reader. The *ADL5511* envelope detector is connected at the output port of the reader. The output port of the envelope detector (tagged as

V_{env}), as well as the tune voltage (tagged as V_{tune}), are managed by the *STM32G070RB* microcontroller. The microcontroller is also in charge of powering all these components. Although the microcontroller is part of the reader electronics, it has not been displayed in the schematic of Fig. 17. Actually, the schematic neither shows the components related to power transform, DAC, USB adapter, among others, because they are not the focus of the work. The fabricated PCB with all these components is shown in Fig. 18(a). The whole electronics system is shown in Fig. 18(b), where a *STM32 Nucleo* board is connected at the output of the designed PCB in order to convert data from USART (Universal Asynchronous Receiver-Transmitter) to SPI (Serial Peripheral Interface) bus. A *MCBID* board is also employed to convert data from SPI to SSI (Synchronous Serial Interface) bus, in order to communicate the data to the external conveyor belt controller. Finally, a mechanical displacement system was designed and implemented, and the photograph of the whole system is depicted in Fig. 18(c).

The procedure to generate and to process the data is constantly repeated, and it is as follows. Firstly, the VCO requires a specific control voltage, V_1 , related to an unmodulated tone at $f_{0,p}$. Such control voltage is set by the microcontroller for a specific time period of $t_s = 30 \mu s$. During this time, the microcontroller is also in charge of retrieving the signal at the envelope (AM) detector output. After the time t_s , the microcontroller changes the control voltage to V_2 for another time period of $2t_s$. This corresponds to a tone at $f_{0,d}$, generated by the VCO. The microcontroller again is reading the signal given by the AM detector. When finishes, the microcontroller sets the control voltage of the VCO to V_3 , (corresponding to the tone at $f_{0,c}$) until $t = 3t_s$. The sweeping time of the three iterations is $3t_s = 90 \mu s$ and during this time the three envelope functions are obtained. Such value of the total time has been chosen taking into account that the time period between two adjacent patches is higher than $90 \mu s$. Actually, this time is ten times higher than the sampling Nyquist criterion. It is to say that the maximum velocity of the microwave encoder is $v_{max} = 4 \text{ mm} / 0.9 \text{ ms} = 4.4 \text{ m/s}$, where the period of the encoder is 4 mm and the time between adjacent patches is set to 10 times $90 \mu s$. However, note that the considered encoder velocity is set to the velocity of the mechanical system. In this case, the reader started moving under the encoder, from right to the left, at a constant velocity of $v = 6.7 \text{ mm/s}$. After some time, the reader stopped ($v = 0 \text{ mm/s}$) for less than one second, and then it changed the direction, from left to the right, at a velocity of $v = -6.7 \text{ mm/s}$.

The functionality of the system was validated by measuring the signal at the envelope detector output, as well as by connecting probes at three external outputs of the microcontroller in order to obtain the digitalized signals for the clock, direction and position tones. The results are shown in Fig. 19, where the gray zone indicates no motion of the reader. At the envelope (AM) detector output (Fig. 19a), the three signals are combined. In the inset, the three intervals t_s ,

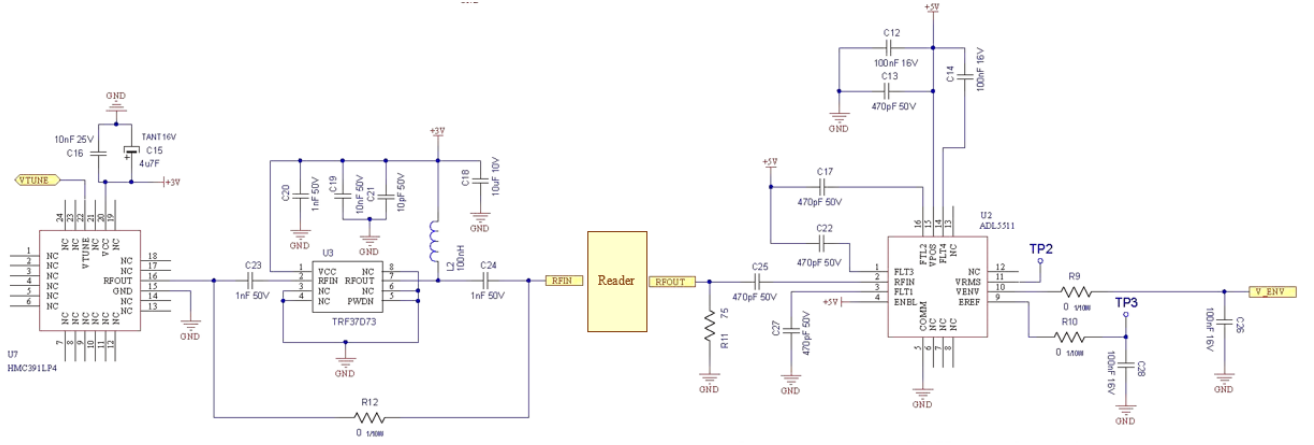


Fig. 17. Schematic of the main components of the reader, concerned the generation and the AM demodulating of the signals.

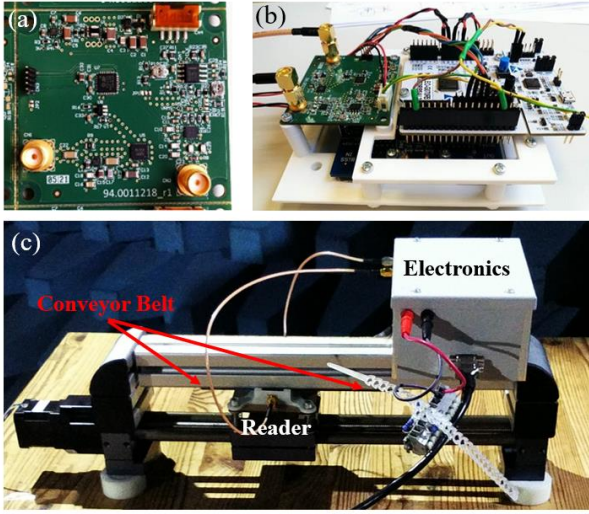


Fig. 18. Photograph of (a) the designed and implemented PCB in charge of generating and processing the three signals, (b) electronics for the full system, which are integrated inside the white box of (c) the linear encoder system used for system validation.

$2t_s$ and $3t_s$ where the voltages are set to V_1 , V_2 and V_3 , respectively, can be seen. Indeed, the inset spans two cycles ($180 \mu s$), corresponding to the black rectangle located around 3 s. The combination of these signals requires the microcontroller, in charge of separating and processing the three signals independently. This process is done internally by the microcontroller, although these three signals have been measured externally to verify the system functionality. Thus, the clock, direction and position signals are plotted in Figs. 19(b), (c) and (d), respectively. During the first two seconds, the reader is displaced from right to left because the rising edge of the clock signal appears before the rising edge of the direction signal (lag). Moreover, while the clock signal is high, the position signal can be obtained. After 2 seconds, the reader stops (during less than one second, as it can be appreciated in Fig. 19). The signals remain inalterable during such period of lack of motion. Then, the reader changes its motion direction because now the rising edge of the clock signal

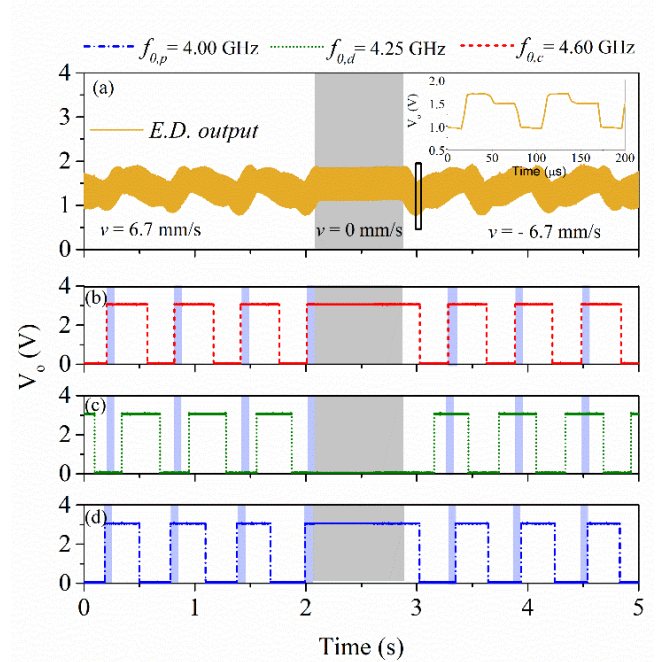


Fig. 19. The measured signal (a) at the envelope detector (ED) output. The inset, corresponding to the black rectangle, shows a small interval of $200 \mu s$ where it can be seen two whole cycles of sweeping time ($2 \times 3t_s = 180 \mu s$). Measured response at the output of the microcontroller corresponding to the digitalized (b) clock signal, (c) direction signal, and (d) position signal.

appears later than the direction signal (lead). As it can be seen, the position signal starts some milliseconds later, because the pulse width is narrower than the clock pulse. For this reason, after reading the rising edge (high state) of the clock, there is some timeframe (of the order of ms). The separation between the adjacent pulses of any signal (i.e., taking as a reference the rising edges) is 0.597 ms , corresponding to a velocity of $|v| = 6.7 \text{ mm/s}$.

After validating the functionality of the whole linear displacement system, the microcontroller was programmed in order to provide the reader position of the encoder by the

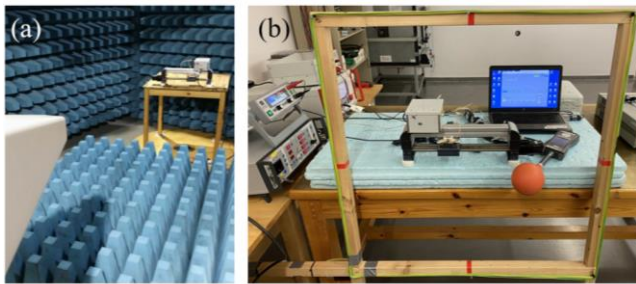


Fig. 20. Photograph of the setup for carrying out the measurements for the (a) radiated, radiofrequency and electromagnetic field immunity, and (b) for the magnetic field immunity.

USART communication interface. Such data information was lately converted to SPI and SSI protocols, by means of the *STM32 Nucleo* and *MCBID* board, respectively, in order to directly communicate the reader position to the conveyor belt controller. This goal was successfully achieved, and the conveyor controller obtained the reader position.

Finally, the system robustness against complex electromagnetic interferences, such as radiofrequency and electromagnetic noise was analyzed (see Fig. 20). Thus, the system was subjected to a set of standard tests for industrial environments (EN 61000-6-2:2019). Specifically, it was tested the radiated, radiofrequency and electromagnetic field immunity (EN 61000-4-3:2006 + A1:2008 + A2:2010), the electrical fast transient/burst immunity (EN 61000-4-4:2012), the surge immunity (EN 61000-4-5:2014/A1:2017), the immunity to conducted disturbances, induced by radiofrequency fields (EN 61000-4-6:2014), and the power frequency magnetic field immunity (EN 61000-4-8:2010). For the first test (EM immunity), the system continued to operate without degradation of performance or loss of functionality from 1 to 6 GHz. However, at certain frequencies, under 1 GHz, when the disturbance was maintained long enough, the system required to be reset. For the second test (burst immunity), the communication with the USB-serial converter was lost during the burst, although the system kept its functionality. For the fourth test (conducted disturbances), the system did not recover when the electric field was applied at frequencies under 80 MHz, and it had to be manually reset. Finally, for the third (surge immunity) and fifth (magnetic field) tests, the system kept its functionality. Thus, after all these tests, it can be concluded that the system operates correctly at the frequencies of interest, although some improvements need to be addressed for some frequencies under 1 GHz and specific components in order to be completely immune to the electromagnetic interferences due to the environment.

V. DISCUSSION

It is worth mentioning that the operation frequencies for the functionality of the system have been selected in the vicinity of 4 GHz as a compromise. Namely, increasing the frequency represents a penalty in terms of the cost of the associated

electronics. On the other hand, if the system works at lower frequencies, the size of the CSRRs increases. Thus, the size of the metallic patches of the encoder also increases, thereby degrading encoder resolution. Thus, it is clear that encoder resolution can be improved by working at higher frequencies, but sacrificing encoder cost.

Other electromagnetic encoders with submillimeter spatial resolution have been reported, but such encoders have been implemented in rigid and low-loss microwave substrates and are not synchronous [19], [28]. Other synchronous electromagnetic encoders, with more than one bit per encoder position have been recently reported [29]-[33]. In these encoders, different inclusions' sizes are considered. Thus, information is encoded in frequency (contrary to the encoders reported in this work, where the state of the single bit per encoder position is determined by the presence or absence of patch in that position). For example, by considering four inclusions sizes, two bits per position are achieved.

In [31]-[33], various position chains are considered as a means to enhance the number of bits per position (up to 8.78 in [32]), but the penalty in this case is the width of the encoder, excessive in certain application. Nevertheless, these encoders may open the path towards the implementation of true absolute electromagnetic encoders, where the unique ID code associated to each position is determined by that position, without the need to read a certain sequence of previous $N - 1$ bits. In [32], the reported resolution is 3 mm (slightly better than in the present work). However, the width of the encoders, implemented by means of narrow strips transversally oriented with regard to the chain axis, is of 15 cm, much larger than the width of the encoders reported in this work. Moreover, the encoders of [32] were implemented in a rigid microwave substrate by means of a drilling machine. By contrast, the encoders of this paper are implemented in a commercial rubber belt, and this forces us to use inclusions' topologies robust against mechanical wearing or friction, i.e., patches, rather than narrow strips. Considering all these aspects, it is believed that the proposed system, with validated functionality in quasi-operational environment, and good performance in terms of resolution (4 mm), is competitive, and can be useful for motion control in industrial scenarios where moving elements are present.

VI. CONCLUSION

In conclusion, a linear displacement sensor system devoted to motion control, consisting of a reader and an encoder, has been proposed and validated. The reader contains two electronic blocks, one of them in charge of generating the interrogation signals, and the other one devoted to processing the output data, plus the sensitive part of the reader (the electromagnetic block). The microwave encoder consists of a conveyor belt where two chains of patches have been printed with silver conducting ink, according to the Bruijn sequence. Before carrying out the whole system validation, several conveyor belts were subjected to tests of mechanical traction, mechanical bending, extreme humidity and temperatures in a climate chamber, and saline salt to test de ink corrosion. After

these tests, the encoders were measured and analyzed, and the results indicated that their functionality was kept essentially unaltered. Thus, a step forward was carried out, consisting in designing and integrating all the electronics, as well as the mechanical guiding system. Finally, the whole linear displacement sensor system was validated by retrieving the conveyor belt position, velocity, and motion direction in a specific designed test.

The advantages of electromagnetic encoders, as those reported in this paper, over other motion sensors are numerous. As compared to other sensing technologies, e.g., optics, microwaves exhibit a superior robustness under operation in harsh and hostile environments, particularly, subjected to pollution, dirtiness, or grease. For example, in optical encoders, it must be ensured that the apertures are clean, so that they can be transparent to the beam generated by the light source (otherwise, system functionality is jeopardized), and this aspect cannot always be guaranteed, especially in industry environments. However, it should be mentioned that optical encoders with very high spatial and angular (in rotary encoders) resolution are commercially available. In this regard, optical encoders are superior to electromagnetic encoders. Nevertheless, for industrial applications involving high dynamic displacement ranges (e.g., conveyor belts, elevators, etc.), a resolution like the one reported in this work (4 mm) is sufficient. As compared to magnetic encoders, the main advantage of the system proposed in this paper, designated as electromagnetic encoder, concerns the fact that neither inductive elements nor magnets are required, and this simplifies the design and reduces the cost. Note that the metallic inclusions (patches) of the electromagnetic encoder are directly printed on the moving element (e.g., the conveyor or elevator belt), provided this behaves as a dielectric material. It should also be mentioned that the associated electronics in the proposed encoder system are relatively simple, since the reader line should be fed by three harmonic signals (managed by a microcontroller), and post processing to retrieve the relevant information (encoder position, velocity and motion direction) does not require complex components, as discussed in the text. Certainly, a multiplicity of other motion sensors based on microwave technology has appeared in the recent literature. Most of such sensors are based on a movable resonator relative to a stator, or reader, typically implemented by means of a transmission line. The working principle in these microwave displacement sensors is radically different to the one that governs electromagnetic encoders. Generally, in those sensors the output variable is the resonance frequency or magnitude in the transmission coefficient of the reader line, which varies when the resonator is in relative motion with regard to the reader line. These sensors, based solely on a single resonant element (at least in most cases) are relatively small, and their design is simple, but their input dynamic range, dictated by the dimensions of the sensing resonator, is very limited, as compared to those dynamic ranges achievable in electromagnetic encoders. Thus, in summary, there is a niche of applications for the proposed electromagnetic encoders, especially in those environments (mostly industrial) where their optical counterparts might experience limitations.

REFERENCES

- [1] E. Eitel, "Basics of rotary encoders: overview and new technologies", *Machine Design Magazine*, 7 May 2014.
- [2] G. K. McMillan, D.M. Considine, Eds., *Process Instruments and Controls Handbook*, Fifth Edition, McGraw Hill 1999, ISBN 978-0-07-012582-7, page 5.26.
- [3] X. Li, J. Qi, Q. Zhang, and Y. Zhang, "Bias-tunable dual-mode ultraviolet photodetectors for photoelectric tachometer," *Appl. Phys. Lett.*, vol. 104, no. 4, pp. 041108-1–041108-4, Jan. 2014.
- [4] J. Naqui, F. Martín, "Application of broadside-coupled split ring resonator (BCSRR) loaded transmission lines to the design of rotary encoders for space applications", *IEEE MTT-S International Microwave Symposium (IMS'16)*, San Francisco, May 2016.
- [5] J. Mata-Contreras, C. Herrojo, and F. Martín, "Application of split ring resonator (SRR) loaded transmission lines to the design of angular displacement and velocity sensors for space applications", *IEEE Trans. Microw. Theory Techn.*, vol. 65, no. 11, pp. 4450–4460, Nov. 2017.
- [6] C. Herrojo, J. Mata-Contreras, F. Paredes, F. Martín, "Microwave encoders for chipless RFID and angular velocity sensors based on S-shaped split ring resonators (S-SRRs)", *IEEE Sensors J.*, vol. 17, pp. 4805–4813, Aug. 2017.
- [7] J. Mata-Contreras, C. Herrojo, and F. Martín, "Detecting the rotation direction in contactless angular velocity sensors implemented with rotors loaded with multiple chains of split ring resonators (SRRs)", *IEEE Sensors J.*, vol.18, no. 17, pp. 7055–7065, Sep. 2018.
- [8] J. Mata-Contreras, C. Herrojo, F. Martín, "Electromagnetic rotary encoders based on split ring resonators (SRR) loaded microstrip lines", *IEEE MTT-S Int. Microw. Symp. (IMS'18)*, Philadelphia, Pennsylvania, Jun. 2018.
- [9] A. Horestani, D. Abbott, and C. Fumeaux, "Rotation sensor based on horn-shaped split ring resonator," *IEEE Sens. J.*, vol. 13, no. 8, pp. 3014–3015, May 2013.
- [10] J. Naqui, and F. Martín, "Transmission lines loaded with bisymmetric resonators and their application to angular displacement and velocity sensors," *IEEE Trans. Microw. Theory Techn.*, vol. 61, no. 12, pp. 4700–4713, Dec. 2013.
- [11] J. Naqui, and F. Martín, "Angular displacement and velocity sensors based on electric-LC (ELC) loaded microstrip lines," *IEEE Sensors J.*, vol. 14, no. 4, pp. 939–940, Apr. 2014.
- [12] A. Ebrahimi, W. Withayachumnankul, S. F. Al-Sarawi and D. Abbott, "Metamaterial-inspired rotation sensor with wide dynamic range," *IEEE Sensors J.*, vol. 14, no. 8, pp. 2609–2614, Aug. 2014.
- [13] J. Naqui, J. Coromina, A. Karami-Horestani, C. Fumeaux, and F. Martín, "Angular displacement and velocity sensors based on coplanar waveguides (CPWs) loaded with S-shaped split ring resonator (S-SRR)", *Sensors*, vol. 15, pp. 9628–9650, 2015.
- [14] V. Sipal, A. Z. Narbudowicz, and M. J. Ammann, "Contactless measurement of angular velocity using circularly polarized antennas", *IEEE Sensors J.*, vol. 15, no. 6, pp. 3459–3466, Jun. 2015.
- [15] A. K. Jha, N. Delmonte, A. Lamecki, M. Mrozowski and M. Bozzi, "Design of microwave-based angular displacement sensor," *IEEE Microw. Wireless Compon. Lett.*, vol. 29, no. 4, pp. 306–308, Apr. 2019.
- [16] A.K. Jha, A. Lamecki, M. Mrozowski, and M. Bozzi, "A Highly Sensitive Planar Microwave Sensor for Detecting Direction and Angle of Rotation", *IEEE Trans. Microw. Theory Techn.*, published online, DOI: 10.1109/TMTT.2019.2957369.
- [17] A.K. Jha, A. Lamecki, M. Mrozowski, M. Bozzi, "A Microwave Sensor with Operating Band Selection to Detect Rotation and Proximity in the Rapid Prototyping Industry", *IEEE Trans. Industrial Electronics*, published online, DOI: 10.1109/TIE.2020.2965464.
- [18] C. Herrojo, F. Muela, J. Mata-Contreras, F. Paredes, F. Martín, "High-density microwave encoders for motion control and near-field chipless-RFID", *IEEE Sensors J.*, vol. 19, pp. 3673–3682, May 2019.
- [19] C. Herrojo, F. Paredes, and F. Martín, "Double-stub loaded microstrip line reader for very high data density microwave encoders", *IEEE Trans. Microw. Theory Techn.*, vol.67(9), pp. 3527–3536, Sep. 2019.
- [20] C. Herrojo, F. Paredes, J. Mata-Contreras, F. Martín, "All-dielectric electromagnetic encoders based on permittivity contrast for displacement/velocity sensors and chipless-RFID tags", *IEEE-MTT-S Int. Microw. Symp. (IMS'19)*, Boston (MA), USA, June 2019.
- [21] C. Herrojo, F. Paredes, and F. Martín, "3D-printed high data-density electromagnetic encoders based on permittivity contrast for motion

>

- control and chipless-RFID", *IEEE Trans. Microw. Theory Techn.*, vol. 68, no. 5, pp. 1839-1850, May 2020.
- [22] F. Paredes, C. Herrojo, F. Martín, "Microwave Encoders with Synchronous Reading and Direction Detection for Motion Control Applications", *2020 IEEE-MTT-S Int. Microw. Symp. (IMS'20)*, Los Angeles, CA, USA, Jun 2020.
- [23] F. Paredes, C. Herrojo, A. Moya, M. Berenguel-Alonso, D. Gonzalez, J. Bruguera, C. Delgado-Simao, and F. Martín, "Electromagnetic Encoders Screen-Printed on Rubber Belts for Absolute Measurement of Position and Velocity", *Sensors*, vol. 22, paper 2044, 2022.
- [24] F. Falcone, T. Lopetegi, J.D. Baena, R. Marqués, F. Martín and M. Sorolla, "Effective negative- ϵ stop-band microstrip lines based on complementary split ring resonators", *IEEE Microw. Wireless Compon. Lett.*, vol. 14, pp. 280-282, Jun. 2004.
- [25] N.C. de Bruijn, "'Acknowledgement of Priority to C. Flye Sainte-Marie on the counting of circular arrangements of $2n$ zeros and ones that show each n -letter word exactly once", *T.H.-Report 75-WSK-06*, Technological University Eindhoven, 1975.
- [26] Z. Zhang, Y. Dong, F. Ni, M. Jin, H. Liu, "A Method for Measurement of Absolute Angular Position and Application in a Novel Electromagnetic Encoder System", *J. Sens.*, pp. 1-10, 2015.
- [27] Z. Zhang, F. Ni, Y. Dong, M. Jin, H. Liu, "A novel absolute angular position sensor based on electromagnetism", *Sens. & Actuators A: Physycal*, vol. 194, pp.196-203, 2013.
- [28] J. Havlíček, C. Herrojo, F. Paredes, J. Mata-Contreras, F. Martín, "Enhancing the per-unit-length data density in near-field chipless-RFID systems with sequential bit reading", *IEEE Ant. Wireless Propag. Lett.*, vol. 18, pp. 89-92, Jan. 2019.
- [29] A. Karami-Horestani, F. Paredes and F. Martín, "Near-Field Hybrid (Time/Frequency Domain) Chipless-RFID System based on Linear Strips Tag", *10th Microwave & RADAR Week*, 12-14 Sep. 2022 Gdansk, Poland.
- [30] A. Karami-Horestani, F. Paredes and F. Martín, "Frequency-coded and programmable synchronous electromagnetic encoders based on linear strips", *IEEE Sensors Lett.*, vol. 6, no. 8, pp. 1-4, Art no. 3501704, Aug. 2022.
- [31] A. Karami-Horestani, F. Paredes and F. Martín, "Near-Field Chipless-RFID System Based on Hybrid Time/Frequency Domain Encoding and Power Splitter Reader", *52nd Europ. Microw. Conf.*, Milan, Italy, 20-25 Sep. 2022.
- [32] A. Karami-Horestani, F. Paredes and F. Martín, "High data density absolute electromagnetic encoders based on hybrid time/frequency domain encoding", *IEEE Sensors J.*, vol. 22, no. 24, pp. 23866-23876, Dec. 2022.
- [33] F. Paredes, A. Karami-Horestani, F. Martín, "Enhancing the bit density in linear electromagnetic encoders for chipless-RFID and motion sensing applications", *European Conference on Antennas and Propagation (EuCAP 2023)*, Florence, Italy, Mar. 27-31, 2023.



Ferran Paredes (M'14-SM'22) received the Telecommunications Engineering degree from the Universitat Autònoma de Barcelona in 2004 and the PhD degree in Electronics Engineering from the same university in 2012. He is working as a Research Assistant at the Universitat Autònoma de Barcelona and his research interests include metamaterial concepts, passive microwaves devices, antennas, and RFID.



Ana Moya is a Senior Scientific in the Functional Printing and Embedded Devices Unit at Eurecat. She received the PhD in Electrical and Telecommunication Engineering in 2017 from UAB. She has an interdisciplinary scientific background, with solid experience in the design and development of electrochemical sensors through printing techniques specially applied on Lab-On-Chip

and Organ-On-Chip systems. Her professional career is focused on the development of printing technologies to produce low cost sensors in flexible substrates which can be of great interest in clinical and environmental analysis.



Miguel Berenguel-Alonso is a Senior Scientist in the Printed Electronics group of Eurecat's Functional Printing and Embedded Devices unit, since 2017. He obtained his PhD in Chemistry in 2017 from UAB, working in the interdisciplinary fields of meso/microfluidics and (bio)sensors. His current research in Eurecat focuses on the development and characterization of sensor systems based on printed electronics, as well as the development of Point of Care devices.



David Gonzalez is electronics engineer in the Hohner Automation R&D department since 2020 with wide experience in both hardware design and firmware developing for microcontrollers. He obtained the degree in 2002 from University of Girona (UdG) and he worked in many industrial sectors as audio for public announcement systems, electric vehicle battery management systems and power electronics.



Pep Bruguera is Industrial Engineer from the University of Girona and Electronic Technical Engineer. His professional career has been developed in Hohner since 1996. He counts on an extensive experience in component designs for industrial automation. As head of the Hohner's R&D&i department, he has led the Company's technological transformation, being responsible for coordinating, developing and supervising product activities of R&D&i, such as the design of innovative processes for the manufacturing of encoders.



Claudia Delgado-Simao have received her PhD in 2011, as a Marie Curie fellow at Institut Ciència de Materials de Barcelona (ICMAB-CSIC), working in the preparation of smart surfaces with tuned optical, magnetic and electric properties. As a post-doctoral researcher, expanded her research fields up to phononic and photonic nanostructures on surface. Currently, is a Senior Scientist and head of the Printed Sensors and Actuators group at Eurecat focusing on developing novel printed devices for innovative solutions in health and environmental applications.

>



Ferran Martín (M'04-SM'08-F'12) received the B.S. Degree in Physics from the Universitat Autònoma de Barcelona (UAB) in 1988 and the PhD degree in 1992. Since 2007 he is Full Professor of Electronics at UAB. He is the head of the Microwave Engineering, Metamaterials and Antennas Group (GEMMA Group) at

UAB, and director of CIMITEC, a Tech-transfer Center. He has authored and co-authored over 650 technical conference, letter, journal papers and book chapters, he is co-author of the book on Metamaterials entitled *Metamaterials with Negative Parameters: Theory, Design and Microwave Applications* (John Wiley & Sons Inc.), author of the book *Artificial Transmission Lines for RF and Microwave Applications* (John Wiley & Sons Inc.), co-editor of the book *Balanced Microwave Filters* (Wiley/IEEE Press), co-author of the book *Time-Domain Signature Barcodes for Chipless-RFID and Sensing Applications* (Springer), and co-author of the book *Planar Microwave Sensors* (Wiley/IEEE Press). Ferran Martín has generated 22 PhDs. Prof. Martín is a member of the IEEE Microwave Theory and Techniques Society (IEEE MTT-S). Among his distinctions, Ferran Martín has received the 2006 Duran Farell Prize for Technological Research, he holds the Parc de Recerca UAB – Santander Technology Transfer Chair, and he has been the recipient of three ICREA ACADEMIA Awards (calls 2008, 2013 and 2018). He is Fellow of the IEEE and Fellow of the IET.